Yorkie and JNK Control Tumorigenesis in Drosophila Cells with Cytokinesis Failure

Gerlach, Stephan U; Eichenlaub, Teresa; Herranz, Héctor

Published in:
Cell Reports

DOI:
10.1016/j.celrep.2018.04.006

Publication date:
2018

Document version
Publisher's PDF, also known as Version of record

Article

Cell Reports

Yorkie and JNK Control Tumorigenesis in *Drosophila* Cells with Cytokinesis Failure

Graphical Abstract

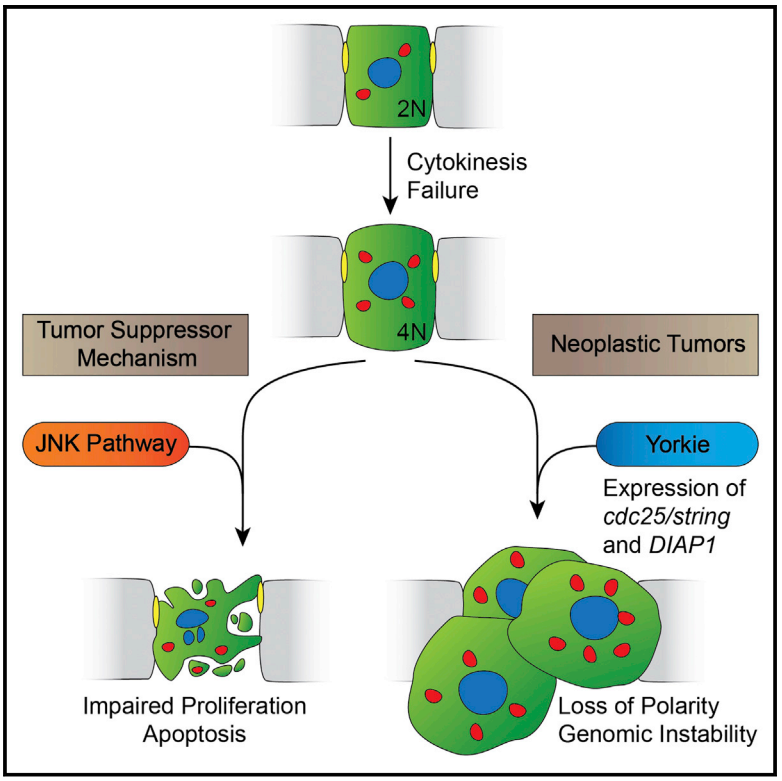

Highlights

- Induction of CF in *Drosophila* epithelial cells
- CF triggers the JNK pathway leading to DIAP1 downregulation and to apoptosis
- Yorkie bypasses cell removal and induces neoplastic tumors in cells with CF
- Yorkie controls the expression of the cell cycle regulator Cdc25/string

Authors

Stephan U. Gerlach, Teresa Eichenlaub, Héctor Herranz

Correspondence

hherranz@sund.ku.dk

In Brief

Cytokinesis failure can be tumorigenic. Gerlach et al. show that JNK represses the expansion of those cells. Yorkie, the *Drosophila* ortholog of YAP and effector of the Hippo pathway, is able to bypass this barrier in cells with cytokinesis defects and cause neoplastic tumors.

Gerlach et al., 2018, Cell Reports *23*, 1491–1503
May 1, 2018
https://doi.org/10.1016/j.celrep.2018.04.006

CellPress

Cell Reports
Article

Yorkie and JNK Control Tumorigenesis in *Drosophila* Cells with Cytokinesis Failure

Stephan U. Gerlach,[1] Teresa Eichenlaub,[1] and Héctor Herranz[1,2,*]
[1]Department of Cellular and Molecular Medicine, University of Copenhagen, Blegdamsvej 3, Copenhagen 2200 N, Denmark
[2]Lead Contact
*Correspondence: hherranz@sund.ku.dk
https://doi.org/10.1016/j.celrep.2018.04.006

SUMMARY

Cytokinesis failure may result in the formation of polyploid cells, and subsequent mitosis can lead to aneuploidy and tumor formation. Tumor suppressor mechanisms limiting the oncogenic potential of these cells have been described. However, the universal applicability of these tumor-suppressive barriers remains controversial. Here, we use *Drosophila* epithelial cells to investigate the consequences of cytokinesis failure *in vivo*. We report that cleavage defects trigger the activation of the JNK pathway, leading to downregulation of the inhibitor of apoptosis DIAP1 and programmed cell death. Yorkie overcomes the tumor-suppressive role of JNK and induces neoplasia. Yorkie regulates the cell cycle phosphatase Cdc25/string, which drives tumorigenesis in a context of cytokinesis failure. These results highlight the functional significance of the JNK pathway in epithelial cells with defective cytokinesis and elucidate a mechanism used by emerging tumor cells to bypass this tumor-suppressive barrier and develop into tumors.

INTRODUCTION

Cytokinesis is the process that physically separates two daughter cells at the end of cell division. In anaphase, the chromosomal passenger complex (a conserved tetrameric complex composed of Aurora B, INCENP, Borealin, and Surviving) localizes to the equatorial cortex and mediates the communication between the spindle midzone and the equatorial cortex. Cytokinesis begins when signaling between the spindle and the cortex generates the formation of an equatorial zone of active RhoA. This directs the formation of the contractile ring, which is composed of F-actin, Myosin II, septin filaments, and the cross-linker anillin. Activated Myosin II drives F-actin sliding and the constriction of the contractile ring. In the last step of cytokinesis, a different system of filaments composed of ESCRT-III proteins controls the physical separation of the two distinct daughter cells (Green et al., 2012). This process ensures the proper partitioning of the nuclear and cytoplasmic cellular contents after mitosis.

Cytokinesis failure (CF) can lead to the duplication of the chromosomal content and the acquisition of extra centrosomes. The presence of extra centrosomes increases the chances of multipolar mitosis in subsequent cell division cycles, whereby chromosomes can be unequally distributed (Ganem et al., 2009; Silkworth et al., 2009). Genomic instability due to unequal chromosome distribution leads to aneuploidy, which has been shown to be oncogenic in animal models (Schvartzman et al., 2010). Remarkably, it is proposed that around 40% of all human cancers have gone through at least one whole genome duplication event during their evolution (Zack et al., 2013). Organisms have therefore acquired mechanisms to restrict cell proliferation after CF.

Given the danger for the organism that CF poses, it has been of interest to determine the molecular basis underlying tumor suppression in this context. Cells with CF have been shown to activate the Hippo pathway, which stabilizes p53 to limit their oncogenic potential (Ganem et al., 2014). Whereas CF in p53-inactive mammary epithelial cells is oncogenic, p53-inactive normal diploid cells do not develop tumors in nude mice (Fujiwara et al., 2005). Thus, CF has been proposed to be causal to tumorigenesis. However, the universal applicability of this tumor-suppressive barrier remains controversial based on the ability of polyploid liver cells to proliferate (Fausto and Campbell, 2003; Uetake and Sluder, 2004).

Here, we have developed a genetic model to induce CF in epithelial cells of *Drosophila*. We have used the fly wing imaginal disc, which is an epithelial monolayer that proliferates actively during larval development, and has been used to model different aspects of tumor progression and metastasis (Herranz et al., 2016). By using this system, we performed a detailed analysis of the consequences of CF. In contrast to human cells, p53 does not have a central role in limiting the oncogenic potential of these cells in the *Drosophila* wing epithelium. Instead, the Jun N-terminal kinase (JNK) pathway restricts the expansion of those cells by repressing the inhibitor of apoptosis DIAP1. Furthermore, the oncogene Yorkie (Yki) is able to induce neoplasia in cells with CF. We identified the cell cycle regulator Cdc25/string as a gene modulated by Yki that, together with DIAP1, can induce the formation of tumors in discs with CF.

RESULTS

Targeted Induction of CF in the *Drosophila* Wing Disc Leads to Apoptosis

The *Drosophila* wing imaginal disc is a highly proliferative epithelium that has proven useful for studying the molecular mechanisms underlying tumorigenesis (Herranz et al., 2016). The

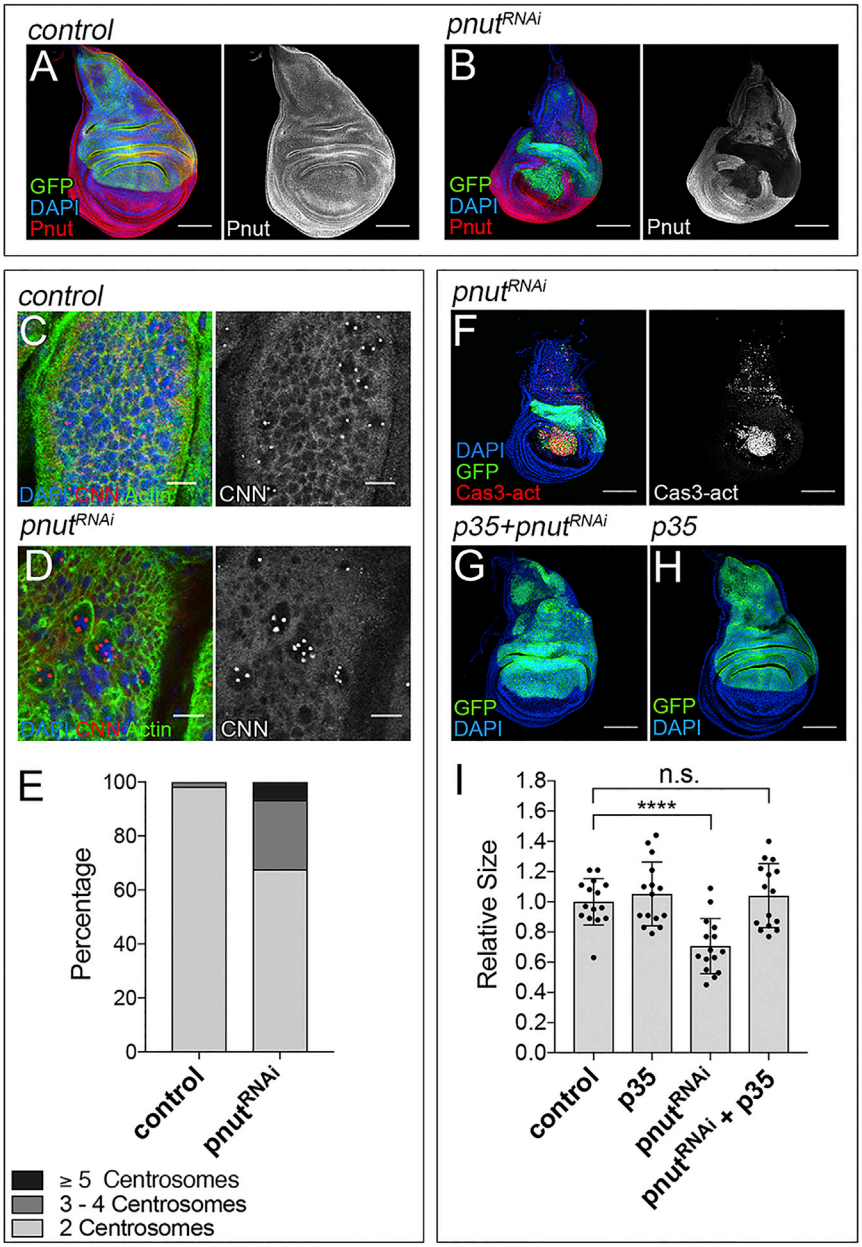

Figure 1. Induction of CF in the Wing Disc Leads to Apoptosis

(A–D) Third-instar wing imaginal discs labeled as indicated in the figure. Scalebar: 100 μm in (A) and (B); 10 μm in (C) and (D).

(E) Quantification of centrosome number of mitotic cells in third-instar wing imaginal discs. Cells were divided in categories, as indicated in the figure. Distribution of centrosome number: control (two centrosomes, 98.33%; three to four centrosomes, 1.67%; five or more centrosomes, 0%); pnut-RNAi (two centrosomes, 67.67%; three to four centrosomes, 25.67%; five or more centrosomes, 6.67%). The majority of cells expressing *pnut-RNAi* had two centrosomes, indicating that *pnut-RNAi* did not block cytokinesis completely. Expressing *pnut-RNAi* generated apoptosis and tissue damage. Given that wing hinge cells are more resistant to apoptosis (Verghese and Su, 2016), images were taken (C and D) and quantification performed (E) in that region of the disc.

(F–H) Third-instar wing imaginal discs labeled as indicated in the figure. Scalebar: 100 μm.

(I) Quantification of GFP-positive area in third-instar wing imaginal discs, normalized to the mean area of the control. Statistical significance determined by unpaired t test (n = 15; n.s., not significant; ****$p < 0.0001$).

Genotypes and duration of transgene expression are described in Supplemental Experimental Procedures.

gene *peanut* (*pnut*) belongs to the Septin family of proteins and is required for cytokinesis in *Drosophila* (Neufeld and Rubin, 1994). Depletion of *pnut* by RNAi in the wing disc leads to CF (Eichenlaub et al., 2016). We made use of the Gal4/UAS binary system to induce CF in the wing disc. We used the *apterous-Gal4* driver (*ap-Gal4*) to direct the expression of the *pnut-RNAi* transgene along with *GFP*. *ap-Gal4* is specifically expressed in the dorsal compartment of the wing disc (Figure 1A, GFP-positive cells). This allows a direct comparison between cells undergoing CF and the adjacent normal cells (GFP-negative) of the ventral compartment, serving as internal control. The protein Pnut can be detected in all the cells of the wing disc (Figure 1A), and the use of *pnut-RNAi* is efficient in depleting Pnut (Figure 1B). The use of an antibody to Centrosomin (CNN), which labels centrosomes in mitosis, revealed the presence of cells with more than the normal two centrosomes in cells expressing *pnut-RNAi* (Figures 1C–1E).

Expression of *pnut-RNAi* in the dorsal cells of the wing disc caused a reduction in tissue size (Figures 1A, 1B, and 1I). This was associated with elevated levels of the activated form of Caspase 3 in dorsal cells (Figure 1F), which reflects cells undergoing apoptosis. Since many of the Pnut-depleted cells appeared to be lost due to apoptosis, we blocked apoptosis by coexpressing the apoptosis inhibitor *p35* together with *pnut-RNAi*. This restored the loss of tissue from the wing disc (Figures 1G and 1I). Expression of *p35* on its own had no effect on wing disc size (Figures 1H and 1I).

CF Leads to Reduced DIAP1 and Apoptosis

In human cells, p53 is stabilized to limit proliferation of cells with CF (Andreassen et al., 2001; Ganem et al., 2014; Kuffer et al., 2013). Consistent with that, cells with CF in the wing disc upregulated p53 (Figure 2A). p53 in *Drosophila* induces apoptosis but does not regulate cell proliferation (Brodsky et al., 2000). To our surprise, apoptosis was not reduced when we expressed *pnut-RNAi* in a *p53*-null mutant background, or together with a

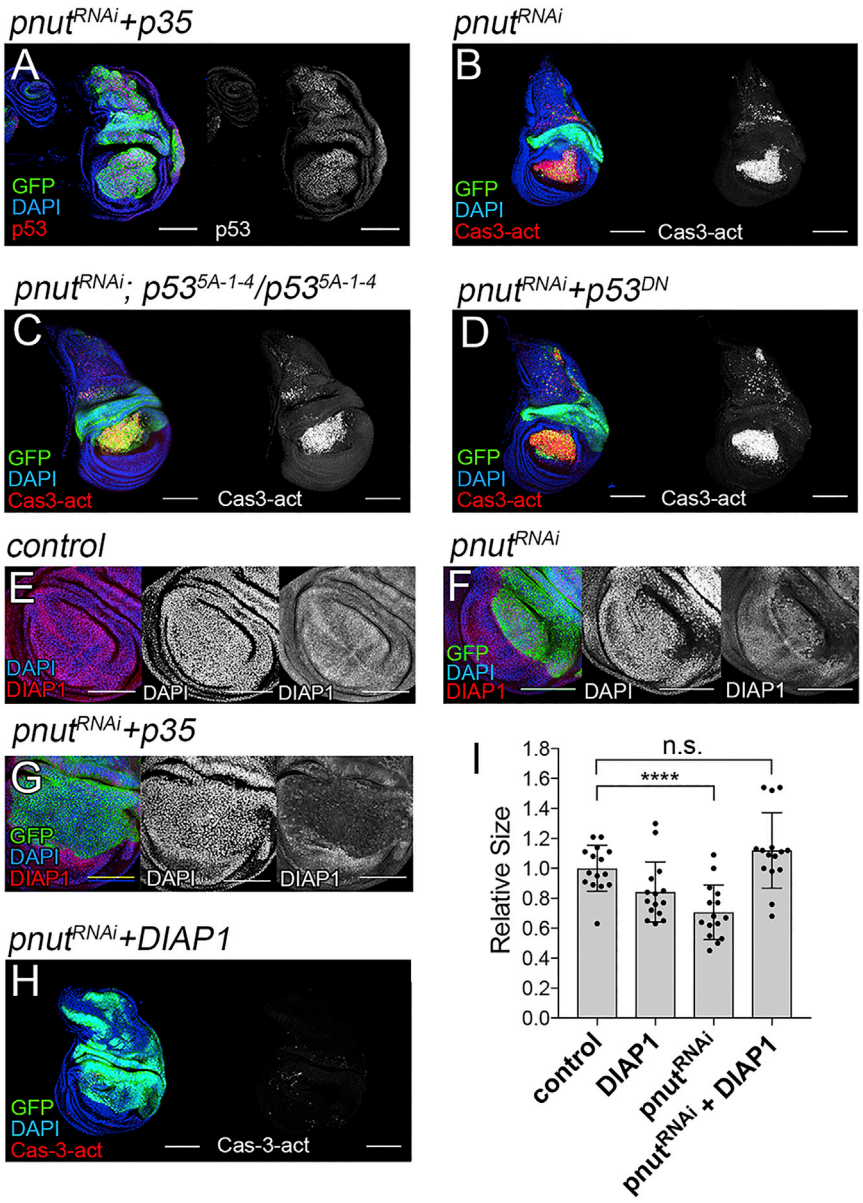

Figure 2. CF Results in DIAP1 Downregulation

(A–H) Third-instar wing imaginal discs labeled as indicated in the figure. Scale bar: 100 μm.

(I) Quantification of GFP-positive area in third-instar wing imaginal discs, normalized to the mean area of the control. Statistical significance determined by unpaired t test (n = 15; n.s., not significant; ****$p < 0.0001$).

Genotypes and duration of transgene expression are described in Supplemental Experimental Procedures.

dominant-negative form of p53 (Figures 2B–2D). This suggests that the induction of apoptosis after CF is independent of p53.

In *Drosophila,* DIAP1 suppresses the caspase cascade and is essential for cell survival (Muro et al., 2002; Wang et al., 1999). Consistently, DIAP1 was observed in all the cells of the normal wing epithelium (Figure 2E). Expression of *pnut-RNAi* led to a reduction in DIAP1 protein in some scattered cells of the wing epithelium (Figure 2F), suggesting that cells with CF downregulate DIAP1 and are eliminated by apoptosis. We reasoned that, if we blocked apoptosis, cells with CF would downregulate DIAP1 but would be maintained in the wing disc, resulting in a higher number of cells with reduced DIAP1 levels. To test this, we analyzed DIAP1 in wing discs coexpressing *pnut-RNAi* and *p35* and found that most of those cells showed a robust decrease in DIAP1 levels (Figure 2G). Expression of *p35* did not affect DIAP1 levels (Figure S1). We studied next whether induction of apoptosis in cells with CF was due to downregulation of DIAP1. Expression of *DIAP1* and *pnut-RNAi* largely suppressed caspase activation and restored tissue size (Figures 2H and 2I), suggesting that CF causes a reduction in DIAP1, and apoptosis.

CF can arise from defects in different elements of the mitotic machinery. To analyze whether downregulation of DIAP1 was a general response to CF, we analyzed DIAP1 in wing discs depleted of different genes involved in cytokinesis. Pebble regulates actomyosin contractile ring assembly (Prokopenko et al., 1999); Diaphanous controls actin cytoskeleton reorganization (Wasserman, 1998); Orbit/MAST is involved microtubule polymerization and spindle assembly (Inoue et al., 2004); and Incenp belongs to the chromosomal passenger complex and plays crucial roles during cytokinesis (Adams et al., 2001; Chang et al., 2006). Notably, depletion of these genes caused CF, when visualized with anti-CNN, and downregulation of DIAP1 (Figure S1). These results suggest that CF in the *Drosophila* wing epithelium results in DIAP1 downregulation, regardless of the specific molecular cause.

Cells with Defective Cytokinesis Upregulate Yki Targets

DIAP1 expression is regulated by the Hippo pathway (Udan et al., 2003; Wu et al., 2003). Hippo signaling controls tissue growth during animal development, and its activation limits cell proliferation and causes apoptosis (Pan, 2010). Besides, core components of the Hippo pathway, including LATS1/2, MOB1, and YAP, control the proper segregation of daughter cells in cytokinesis (Brace et al., 2011; Bui et al., 2016; Florindo et al., 2012; Mukai et al., 2015; Yabuta et al., 2016). Interestingly, CF causes activation of the Hippo pathway in a human epithelial cell model (Ganem et al., 2014).

In *Drosophila*, activation of the Hippo pathway represses the cotranscriptional activator Yki. As a consequence, the expression of Yki target genes such as *DIAP1* are downregulated. We studied whether CF affected Yki activity, as observed for the Yki human ortholog, YAP (Ganem et al., 2014). We analyzed the expression of the Yki-target genes: *DIAP1-lacZ*, *Cyclin E-lacZ*, *Expanded-lacZ*, *bantam-lacZ*, and *four jointed-lacZ* (Brennecke et al., 2003; Cho et al., 2006; Hamaratoglu et al., 2006). To limit tissue damage caused by apoptosis, we expressed *p35* together with *pnut-RNAi*. This facilitated the analysis of Yki target genes. To our surprise, even though DIAP1 protein levels were reduced in cells with CF, *DIAP1-lacZ* was upregulated (Figures 3A and 3B). This was confirmed by *in situ* hybridization (Figure 3C). Consistent with this, the expression of the Yki-target genes *Cyclin E-lacZ*, *Expanded-lacZ*, *bantam-lacZ*, and *four jointed-lacZ*, was increased in cells with CF (Figures 3D–3G). Expression of *p35* on its own caused a reduction in *Cyclin E-lacZ*, yet *p35* did not affect the expression of the other Yki-target genes analyzed (Figure S2). In sum, contrary to what has been observed in human cells where CF leads to repression of the Yki human ortholog YAP (Ganem et al., 2014), CF in the wing imaginal epithelium results in Yki upregulation.

JNK Pathway Regulates DIAP1 Protein after CF

Although the expression of *DIAP1* was increased in cells with CF, DIAP1 protein was reduced in those cells, suggesting that DIAP1 was repressed posttranscriptionally. The JNK pathway can regulate DIAP1 posttranscriptionally (Kanda and Miura, 2004). JNK is activated in response to different types of stress and is a major proapoptotic factor in *Drosophila*. JNK activation induces the expression of members of the *reaper*, *hid*, *grim* family of proapoptotic genes. Those proteins bind DIAP1 and induce its degradation. Thereby, they release caspase inhibition and induce cell death (reviewed in Hay and Guo, 2006).

We first analyzed whether JNK was active in cells with CF. To monitor JNK activity, we used an antibody against the JNK target Mmp1 (Uhlirova et al., 2005), a transgenic reporter of JNK activity consisting of binding sites for the JNK pathway transcription factor AP1 (TRE-RFP) (Chatterjee and Bohmann, 2012), and an antibody that recognizes the phosphorylated and active form of JNK (pJNK) (Willsey et al., 2016). Cells expressing *pnut-RNAi* upregulated Mmp1, TRE-RFP, and pJNK (Figures 3H–3J), indicating that the JNK pathway was active in cells with CF. We used a dominant-negative version of JNK (*bsk-DN* in *Drosophila*) to investigate whether DIAP1 downregulation was JNK dependent. Interestingly, DIAP1 protein levels were partially restored when we inhibited the JNK pathway by expressing *bsk-DN* in cells with CF (Figure 3K). Consistently, apoptosis was reduced in those wing discs, as compared to wing discs expressing *pnut-RNAi* on its own (Figures 3L–3N). Mmp1 expression was blocked upon expression of *bsk-DN*, indicating that this transgene was efficient in downregulating JNK activity (Figures 3L and 3M). Together, these findings indicate that JNK triggers apoptosis by repressing DIAP1 protein in cells with CF.

Reduced Proliferation in Cells with Defective Cytokinesis

Cells with CF arrest in G1 in a p53-dependent manner in murine models (Andreassen et al., 2001; Lanni and Jacks, 1998; Minn et al., 1996). However, p53 does not seem to play a central role in response to CF in the wing epithelium of *Drosophila*. We made use of the fluorescence ubiquitin cell cycle indicator (FUCCI) technology (Sakaue-Sawano et al., 2008) to visualize cell cycle phasing in the wing disc with CF. The *Drosophila* FUCCI system (Fly-FUCCI) labels cells in G1 phase in green and cells in S-phase in red, and cells in G2 phase appear yellow (Figure 4A) (Zielke et al., 2014). Expression of *Fly-FUCCI* under the control of *ap-Gal4* in otherwise-normal wing discs showed cells labeled in different colors (red, green, and yellow), indicating the presence of cells in different phases of the cell cycle (Figures 4B and 4F).

Cells with CF downregulated DIAP1 and were eliminated by apoptosis. To interrogate how the cell cycle was regulated in those cells, we prevented apoptosis by expressing *DIAP1*. In that context, most of the tetraploid cells were labeled in yellow, which indicated that they were not arrested in G1 and progressed to G2 (Figures 4C, 4F, and S3). Inhibition of apoptosis by expression of *p35* led to comparable results (Figures 4D, 4F, and S3). The number of cells labeled in red (S-phase) was dismissible and was not shown in this analysis.

Expression of *pnut-RNAi* on its own led to massive apoptosis (Figure 1). Notably, the number of tetraploid cells in those wing discs was reduced as compared to wing discs expressing *pnut-RNAi* and repressing apoptosis (*pnut-RNAi+DIAP1,* or *pnut-RNAi+p35*) (Figures 4E and 4F). This supports the notion that tetraploid cells generated by CF are eliminated by apoptosis.

In contrast to mammalian cells, tetraploid cells in the wing disc were not arrested in G1. To test whether these cells were arrested in G2, we labeled them with the mitotic marker PH3. We detected the presence of PH3-positive cells (Figure 4G). This, together with the observation of cells with more than four centrosomes in discs expressing *pnut-RNAi* (Figure 1), indicates that cells with CF in the wing epithelium are not arrested in G2 and can progress to mitosis. 5-Ethynyl-2′-deoxyuridine (EdU) labels cells in S-phase and allows for an accurate quantification of proliferating cells. Cells coexpressing *pnut-RNAi* and *p35* showed a strong reduction in the number of EdU-positive cells, as compared to control wing discs (Figures 4H and 4I), indicating that cells with CF proliferate poorly.

Signals Inducing Tumor Formation after CF

Induction of CF in *p53* mutant mouse mammary epithelial cells produces malignant tumors in nude mice (Fujiwara et al., 2005). In contrast to that, CF in wing discs depleted of p53 did not develop tumors in the wing primordia of *Drosophila* (Figures 2C and 2D). Intrigued by this, we sought to identify potential signals inducing tumorigenesis in this context. We performed a screen where tumor suppressors were inactivated by RNAi in wing discs with CF, and we tested for the formation of tumors (the list with the tumor suppressors tested are listed in Table S1). Among the wing discs analyzed, only the ones depleting the *warts* tumor-suppressor gene grew as tumors in a context

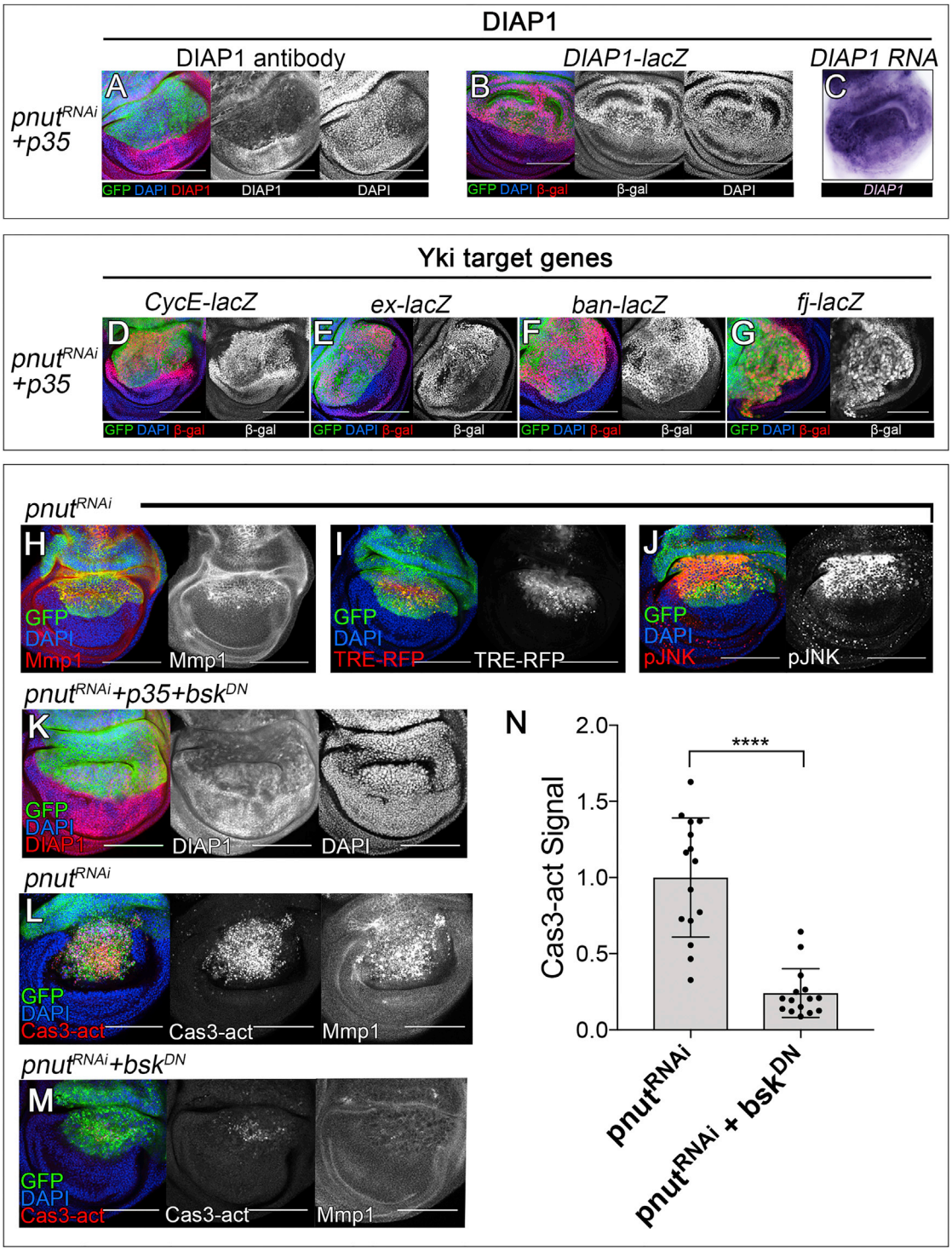

Figure 3. JNK Downregulates DIAP1 in Cells with CF

(A–M) Third-instar wing imaginal discs labeled as indicated in the figure. Scalebar: 100 μm.

(N) Quantification of activated form of Caspase 3 signal in third-instar wing imaginal discs, normalized to the mean signal of "*pnut-RNAi*." Statistical significance was determined by unpaired t test (n = 15; ****$p < 0.0001$).

Genotypes and duration of transgene expression are described in Supplemental Experimental Procedures.

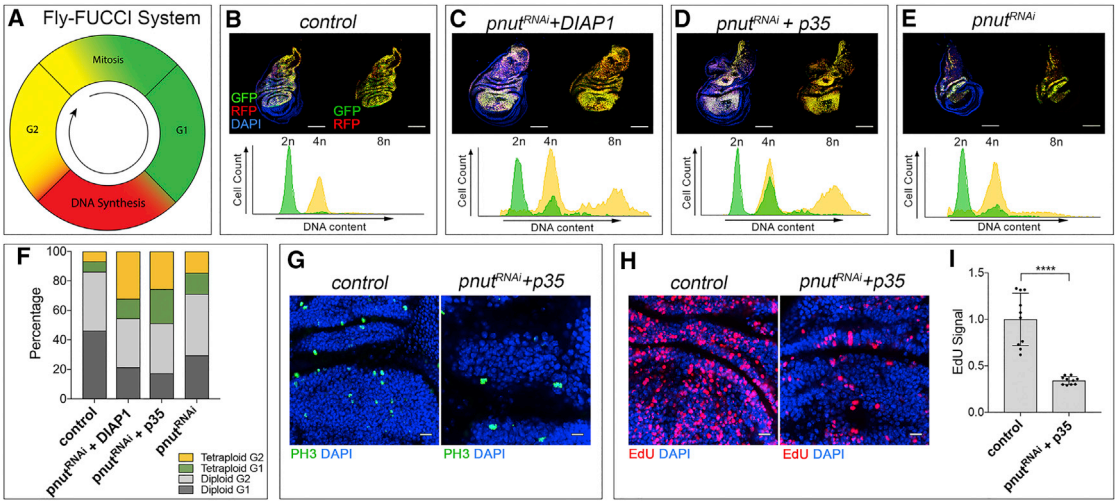

Figure 4. Cells with CF Show Defects in Proliferation

(A) Model illustrating the fly-FUCCI system. Cells in G1 are labeled in green, cells in S-phase are labeled in red, and cells in G2 appear yellow.

(B–E) Third-instar wing imaginal discs labeled as indicated in the figure. Scalebar: 100 μm. FACS was used to quantify cells in G1 and G2. FACS profiles are shown. Diploid (2n), tetraploid (4n), and octaploid (8n) DNA content is indicated. Cells in G1 are shown in green, and cells in G2 are shown in yellow.

(F) Quantification of cell cycle phases in diploid and tetraploid cells in third-instar wing imaginal discs. Cells were divided in categories, as indicated in the figure. Distribution of cell cycle phases in diploid and tetraploid cells: control (diploid G1, 46.17%; diploid G2, 40.17%; tetraploid G1, 6.91%; tetraploid G2, 6.75%); pnut-RNAi + DIAP1 (diploid G1, 21.40%; diploid G2, 33.16%; tetraploid G1, 13.28%; tetraploid G2, 32.16%); pnut-RNAi + p35 (diploid G1, 17.33%; diploid G2, 33.94%; tetraploid G1, 23.17%; tetraploid G2, 25.56%); pnut-RNAi (diploid G1, 29.60%; diploid G2, 41.68%; tetraploid G1, 14.31%; tetraploid G2, 14.41%).

(G and H) Third-instar wing imaginal discs labeled as indicated in the figure. Scalebar: 10 μm.

(I) Quantification of EdU signal in third-instar wing imaginal discs, normalized to the mean area of the control. Statistical significance determined by unpaired t test (n = 10; ****$p < 0.0001$).

Genotypes and duration of transgene expression are described in Supplemental Experimental Procedures.

of CF. Those wing discs were not reduced in size when compared to wing discs depleting the different tumor suppressor on their own (Figures 5A–5C and S4).

Warts is a kinase in the Hippo pathway that phosphorylates and inactivates Yki. Consistently, coexpression of *yki* and *pnut-RNAi* resulted in the formation of tumors (Figure 5D). *yki* is an oncogene that induces hyperplastic tissue overgrowth in the wing disc. We analyzed whether the oncogenic potential of Yki in cells with CF reflected a general response to oncogene activation or was specific for Yki. We combined the expression of *pnut-RNAi* with transgenes expressing different oncogenes such as *EGFR*, *RasV12*, *Notch*, *decapentaplegic*, *wingless*, and *PI3K* (reviewed in Herranz et al. [2016]) (Figures 5E, 5F, and S4). Remarkably, *yki* and Ras^{V12} were the only oncogenes that induced the formation of tumors in cells depleted of Pnut (Figures 5D–5F and S4).

Consequently, we asked whether the effect of Yki was specific for Pnut depletion or a general consequence of CF. Tumors were observed when *yki* was coexpressed with *UAS-RNAi* transgenes targeting the cytokinesis genes *Orbit/MAST*, *diaphanous*, *pebble*, and *Incenp* (Figure S5). Collectively, these data suggest that *yki* overexpression drives tumor formation after CF.

Yki Drives the Formation of Neoplastic Tumors in Wing Discs with Defects in Cytokinesis

Cancer involves the cooperation of different mutations to drive malignancy from benign tumors. We determined next whether tumors driven by Yki in a context of CF were benign overproliferating tissues or showed malignant features.

Larvae expressing *yki* under the control of *ap-Gal4* entered pupariation and died as pupae. In contrast, larvae coexpressing *yki* and *pnut-RNAi* did not pupate and, instead, continued to grow to form giant larvae (Figure 6A). We analyzed wing discs expressing *yki* with and without *pnut-RNAi* 4 days after the induction of transgene expression. Those wing discs were comparable in size, indicating that the wing discs grow at a similar rate (Figure 6B). However, while larvae with wing discs expressing *yki* entered pupariation, the tumors coexpressing *yki* and *pnut-RNAi* continued growing beyond that time point and led to the formation of giant larvae (Figures 6A and 6B), which is characteristic of larvae with malignant tumors (Bilder, 2004).

In carcinomas, one of the primary diagnostic features of malignancy is a pronounced disorganization of epithelial architecture. *yki* overexpression induced tissue overgrowth, yet the tissue maintained the normal epithelial organization, as revealed by the polarity marker Discs large (Figure 6C). Epithelial polarity was compromised in tumors expressing *yki* and *pnut-RNAi*, reflected by the mislocalization of Discs large (Figure 6D). This suggests that tumors grow as neoplastic tumors, which can result from loss of epithelial polarity (Bilder, 2004).

Malignant fly tumors express the secreted *matrix metalloproteinase 1* (*Mmp1*). Mmp1 degrades the basement membrane of the imaginal disc, allowing tumor cells to migrate and invade (Beaucher et al., 2007; Uhlirova and Bohmann, 2006). In normal

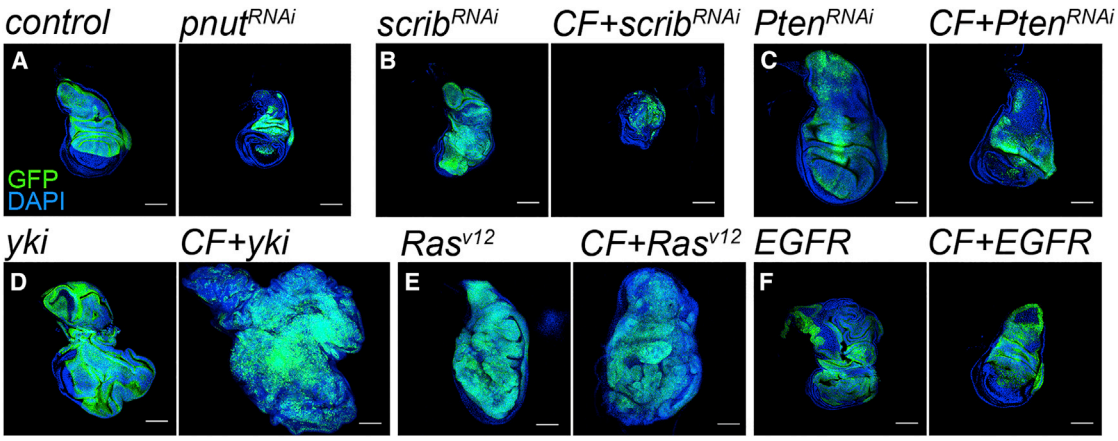

Figure 5. Yki and Ras-V12 Drive Tumor Formation after CF

(A–F) Third-instar wing imaginal discs labeled as indicated in the figure. Scalebar: 100 μm. Genotypes and duration of transgene expression are described in Supplemental Experimental Procedures.

wing discs, *Mmp1* is not expressed in the proliferating epithelium and is only detected in the wing disc trachea (Figure 6E). Expression of *yki* led to *Mmp1* upregulation in a group of cells of the wing disc (Figure 6F). The tumors expressing *yki* and *pnut-RNAi* showed a robust increase in the levels of Mmp1 protein (Figure 6G). As shown previously, Mmp1 expression was observed in wing discs expressing *pnut-RNAi* on its own (Figure 6H). This indicates that CF is sufficient to induce the expression of the proinvasive marker Mmp1.

We studied the invasive potential of those tumor cells. The *Drosophila* wing disc is subdivided into compartments (Mann and Morata, 2000). Cells of different compartments do not mix during normal development, and this can be used to model cell invasion (Vidal et al., 2006). We used the posterior-specific Gal4 driver, *hedhehog-Gal4* (*hh-Gal4*) (Figure 6I), to determine whether tumor cells could migrate through the anterior-posterior compartment boundary. Expression of *yki* under the control of *hh-Gal4* induced tissue overgrowth (Figure S5), but these cells did not mix with cells of the anterior compartment (Figures 6J and 6O). Interestingly, posterior cells coexpressing *yki* and *pnut-RNAi* were observed in the anterior compartment (Figures 6K–6O). This suggests that tumors expressing *yki* and *pnut-RNAi* are invasive.

Centrosomes are the main microtubule organizing centers in animal cells, and they are replicated during the cell cycle to form the poles of the mitotic spindle. CF, in addition to whole genome duplication, leads to the acquisition of extra centrosomes. We detected the presence of cells with supernumerary centrosomes in the tumors expressing *yki* and *pnut-RNAi*. We observed that larger cells with bigger nuclei and higher number of centrosomes are formed during tumor progression (Figures 6P–6R and S5). The presence of supernumerary centrosomes can lead to genome instability and aneuploidy, which is a common feature of carcinomas.

We obtained comparable results in the eye epithelium, suggesting that the induction of neoplasia by Yki in cells with CF might be a general phenomenon and not a wing-specific outcome (Figure S5).

In summary, the formation of giant larvae, defects in polarity, expression of the proinvasive marker Mmp1, invasiveness, and induction of genomic instability, suggest that tumors expressing *yki* and *pnut-RNAi* have acquired malignant features.

Yki Regulates the Expression of *Cdc25/string*

Previous studies have reported that preventing apoptosis in aneuploid cells can lead to tumor formation in the wing disc (Dekanty et al., 2012; Morais da Silva et al., 2013). Although Yki represses apoptosis by inducing the expression of *DIAP1*, blocking apoptosis in cells with CF was not sufficient for tumorigenesis (Figure 4). We observed that most of the tetraploid cells coexpressing *pnut-RNAi* and *DIAP1* were found in G2. This suggests that Yki, in addition to prevent apoptosis by regulating *DIAP1*, should promote G2/M transition to drive cell proliferation and tumor formation.

The phosphatase Cdc25 is the main activator of G2/M transition in eukaryotic cells (Bouldin and Kimelman, 2014), and expression of *string* (*stg*), the *Drosophila* ortholog of Cdc25, is effective in driving G2/M progression. Cells coexpressing *stg* and *fly*-FUCCI appeared green (cells in G1) or red (cells in S-phase) (Figure S6). *stg* accelerated G2/M progression but did not affect the growth of the wing disc (Figure 7F). Wing disc cells compensate alterations in the length of the cell cycle phases by altering the lengths of the other phases. This homeostatic mechanism ensures that, when the cell cycle is perturbed, the rates of cell proliferation are not altered (Reis and Edgar, 2004).

We analyzed whether Yki regulated the expression of *stg* in the wing epithelium. To monitor *stg* expression, we made use of the *stg-lacZ* enhancer trap reporter *P{PZ}stg01235*, and RNA *in situ* hybridization. *stg* is expressed ubiquitously in the wing disc, showing higher expression levels in cells close to the anterior-posterior and dorsal-ventral boundaries (Figure 7A). *yki* overexpression resulted in increased *stg* expression (Figure 7B). Consistently, depletion of Yki led to a reduction in the expression of *stg* (Figure 7C).

Yki is a cotranscriptional activator and functions in concert with DNA-binding transcription factors like Scalloped (Sd) to

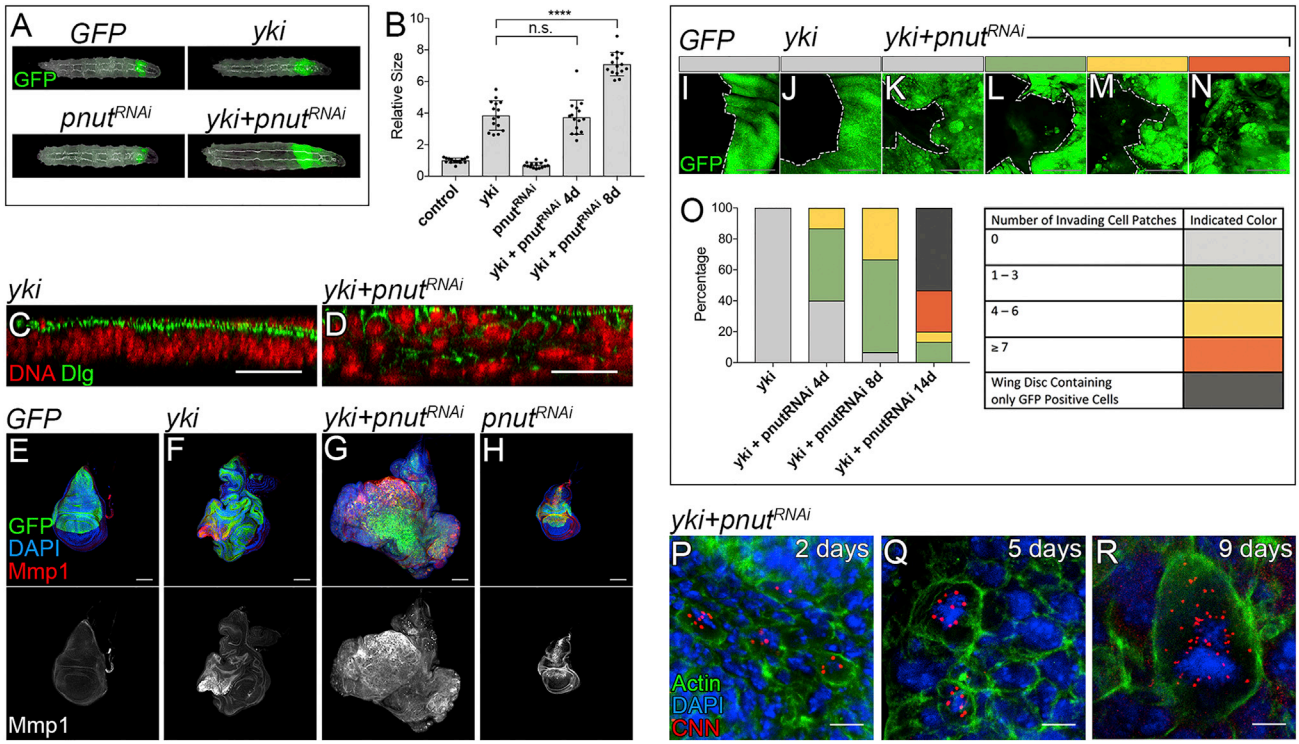

Figure 6. Yki Induces the Formation of Neoplastic Tumors in Cells with CF

(A) Low-magnification images of whole larvae of the genotypes indicated.

(B) Quantification of GFP-positive area in third-instar wing imaginal discs, normalized to the mean area of the control. Statistical significance determined by unpaired t test (n = 15; n.s., not significant; ****p < 0.0001).

(C–H) Third-instar wing imaginal discs, labeled as indicated in the figure. Cross-section is shown in (C) and (D). Scalebar: 100 μm.

(I–N) Third-instar wing imaginal discs, labeled as indicated in the figure. Anterior and posterior compartment is shown (border marked with white line). Pictures represent the categories for quantification of invading cell patches (shown in O): no invading cell patches (I–K); one to three invading cell patches (L); four to six invading cell patches (M); and seven or more invading cell patches (N). Scalebar: 100 μm.

(O) Quantification of invading cells from the posterior to anterior compartment in third-instar wing imaginal discs. Wing imaginal discs were divided in categories, as indicated in the figure. Distribution of invading cells: yki (0 invaded cell patches, 100%); yki + pnut-RNAi 4d (0 invaded cell patches, 40%; one to three invaded cell patches, 47%; four to six invaded cell patches, 13%); yki + pnut-RNAi 8d (0 invaded cell patches, 7%; one to three invaded cell patches, 60%; four to six invaded cell patches, 33%); yki + pnut-RNAi 14d (one to three invaded cell patches, 13%; four to six invaded cell patches, 7%; seven or more invaded cell patches, 27%; wing disc containing only GFP-positive cells, 53%).

(P–R) Third-instar wing imaginal discs, labeled as indicated in the figure. Scalebar: 10 μm.

Genotypes and duration of transgene expression are described in Supplemental Experimental Procedures.

induce tissue growth (Goulev et al., 2008; Wu et al., 2008; Zhang et al., 2008). Interestingly, a recent paper by Georg Halder's group (Atkins et al., 2016) generated a list of high-confidence Yki-Sd target genes that included *stg* as a gene potentially regulated by Yki-Sd. Together, these observations suggest that *stg* is a direct Yki-Sd target gene.

Yki Drives Tumor Formation by Regulating *Cdc25/string* and *DIAP1*

Expression of *yki* in cells with CF upregulated *stg* and *DIAP1* (Figures 7D and 7E). We reasoned that, in order to form tumors, Yki could limit apoptosis by inducing *DIAP1* and promote cell cycle progression by upregulating *stg*. To test whether upregulation in *DIAP1* and *stg* was sufficient to drive tumor formation, we substituted the *UAS-yki* transgene for *UAS-DIAP1* and *UAS-stg.* Even though coexpression of *DIAP1* and *stg* did not increase the size of normal wing discs, expression of *stg* and *DIAP1* in cells with CF was sufficient to drive the formation of tumors (Figures 7F and 7G).

The expression of *stg* was sufficient to overcome the delay in G2 observed in wing discs expressing *pnut-RNAi* and *DIAP1* (Figure S6). Interestingly, the cell cycle pattern observed in wing discs expressing *pnut-RNAi, DIAP1*, and *stg*, was different to the one in wing discs expressing *pnut-RNAi*, and *yki* (Figure S6). This suggests that other Yki target genes, in addition to *DIAP1* and *stg*, are contributing to the formation of the tumors. Yki can modulate G1/S progression by regulating target genes such as *Cyclin E* (Huang et al., 2005), and this might explain the differences observed in the cell cycle pattern.

JNK Suppresses *Cdc25/string* Overexpression in Cells with Cytokinesis Defects

As observed for other Yki-target genes, cells coexpressing *pnut-RNAi* and *p35* upregulated the expression of *stg* (Figures 7H and

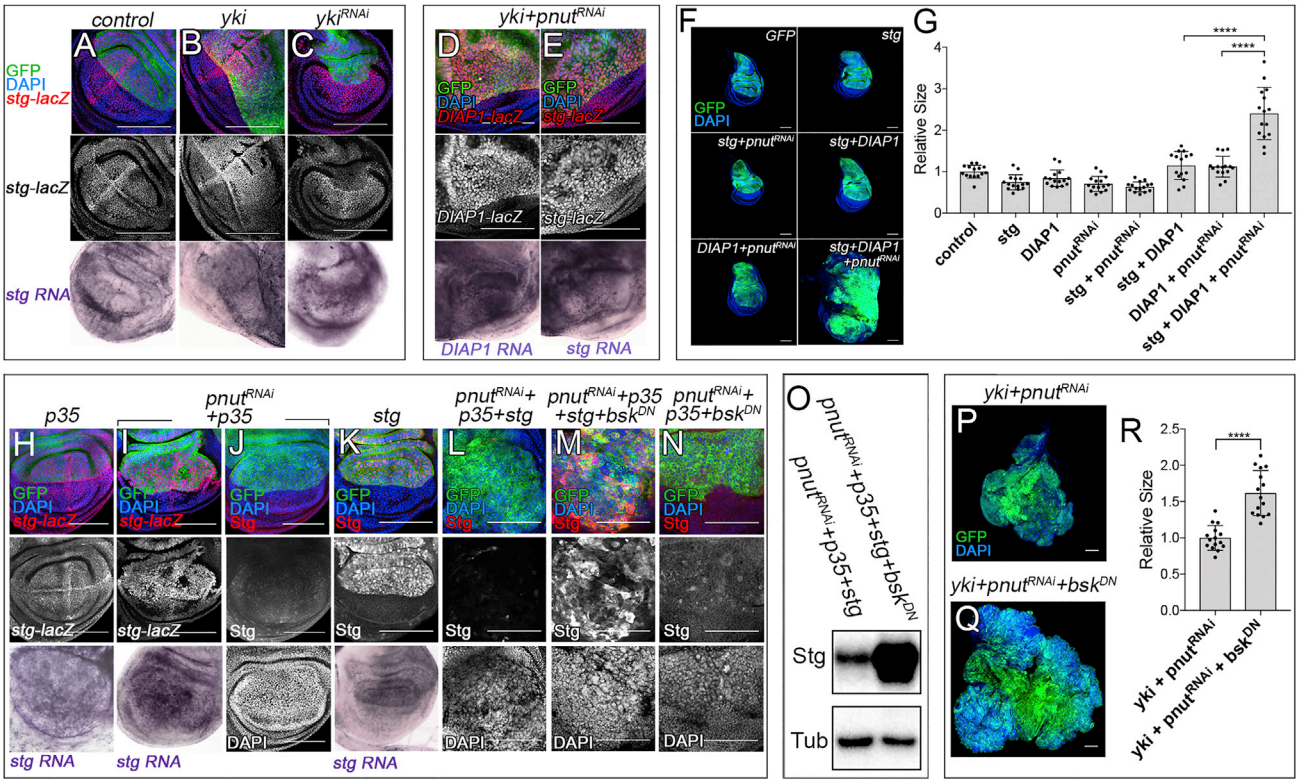

Figure 7. Yki Regulates the Expression of *string*, Which Promotes Tumor Formation

(A–E) Third-instar wing imaginal discs, labeled as indicated in the figure. Scalebar: 100 μm.

(G) Quantification of GFP-positive area in third-instar wing imaginal discs, normalized to the mean area of the control. Statistical significance determined by unpaired t test (n = 15; ****p < 0.0001).

(H–N) Third-instar wing imaginal discs, labeled as indicated in the figure. Scalebar: 100 μm.

(O) Western blot showing Stg protein in third-instar wing imaginal discs of the genotypes indicated. Tub was used as a loading control.

(P and Q) Third-instar wing imaginal discs, labeled as indicated in the figure. Scalebar: 100 μm.

(R) Quantification of GFP-positive area in third-instar wing imaginal discs, normalized to the mean area of *yki+pnut*^{RNAi}. Statistical significance determined by unpaired t test (n = 15; ****p < 0.0001).

Genotypes and duration of transgene expression are described in Supplemental Experimental Procedures.

7I). However, Stg protein levels were not increased in those wing discs (Figure 7J). To our surprise, overexpression of *stg* in a context of CF did not result in an increase in Stg protein, as compared to wing discs expressing *stg* in an otherwise-normal background (Figures 7K and 7L). This suggested that, as observed for DIAP1, Stg might be regulated posttranscriptionally in cells with CF. Cells with CF activate the JNK pathway, and interestingly, JNK has been shown to repress Cdc25b and Cdc25c in human cell lines (Gutierrez et al., 2010; Uchida et al., 2009). Remarkably, repression of JNK in wing discs expressing *stg* in a context of CF, led to a robust increase in Stg protein (Figure 7M; compare with Figure 7L—those discs were labeled in parallel and imaged under the same conditions). This suggests that JNK is a central regulator of Stg in cells with CF. To confirm that JNK limits Stg in cells with CF overexpressing *stg*, we measured Stg protein levels by western blot in the genetic conditions shown in Figures 7L and 7M. Consistent with our previous observations, we found a dramatic increase in Stg protein levels in wing discs suppressing JNK (Figure 7O). However, we did not detect an overt increase of Stg protein levels in wing discs expressing *pnut-RNAi*, *p35*, and *bsk-DN* (Figure 7N). JNK was efficient in repressing Stg in wing discs with CF and *stg* overexpression. This suggests that JNK could behave as a tumor suppressor in the context of CF. Consistently, blocking JNK activity in tumors expressing *yki* and *pnut-RNAi* led to an increase in tumor size (Figures 7P–7R), supporting that JNK has a tumor-suppressive role in cells overexpressing *yki* in a context of CF.

DISCUSSION

Proliferation of cells with defects in cell division creates an unstable situation that leads to genomic instability, which is a common feature in cancer. Mechanisms to eliminate abnormal cells are important to prevent carcinogenesis. Mammalian cells with genomic instability are eliminated by apoptosis in a p53-dependent manner (Burds et al., 2005; Li et al., 2010). In contrast to that, our current study shows that induction of CF in the *Drosophila* wing primordia leads to p53-independent apoptosis. We show that wing disc cells with CF are eliminated as a

consequence of JNK activation and DIAP1 downregulation. In good agreement with our results, induction of genomic instability in the *Drosophila* wing disc by affecting genes involved in spindle assembly, spindle assembly checkpoint, and chromosome condensation, also results in p53-independent and JNK-dependent apoptosis (Dekanty et al., 2012; Morais da Silva et al., 2013). Interestingly, induction of chromosomal instability in those contexts induces neoplastic growth, when cells are prevented from apoptosis (Dekanty et al., 2012; Morais da Silva et al., 2013). In contrast, blocking apoptosis in cells with CF is not sufficient to induce tumor formation.

In mammals, CF leads to activation of the Hippo pathway that results in the repression of the oncogene YAP (Ganem et al., 2014). In contrast to that, the results presented here show that cells with CF in the *Drosophila* wing primordia upregulate the expression of Yki-target genes. This suggests that Yki activity is upregulated after CF, and evidence that activation of the Hippo pathway in this context might not be a universal response. Furthermore, while mammalian cells with CF arrest in G1 in a p53-dependent manner (Andreassen et al., 2001; Lanni and Jacks, 1998; Minn et al., 1996), *Drosophila* epithelial cells progress to G2. This reinforces the notion that p53 in flies has a different function to the one described in mammals. In sum, the response to CF seems to be different in mammals and *Drosophila*, which suggests that different organisms might use distinct molecular mechanisms to control the propagation of these cells.

In order to prevent genomic instability, cells also use other mechanisms such as cell cycle checkpoints. Cancer cells need to undergo genetic changes to escape those tumor-suppressive barriers. Thus, the initiation of carcinogenesis can occur through the activation of an oncogene that, even when those checkpoints are active, induces cell proliferation and the expansion of precancerous cells. In fact, the dysfunction of cell cycle regulators is frequently associated with uncontrolled cell proliferation observed in cancer. We show that Yki is able to induce the formation of tumors in a context of CF and identify the cell cycle regulator *Cdc25/stg* as Yki-target gene. Our results show that upregulation of Cdc25/stg and inhibition of apoptosis in cells with CF can trigger cell cycle progression and the formation of tumors in *Drosophila* epithelial cells. Interestingly, the ability of Cdc25/stg to drive tumorigenesis appears to be context dependent. Even though *Cdc25/stg* acts as a potent oncogene when overexpressed in cells with CF, it does not affect the growth of the normal wing epithelium.

The role of the JNK pathway in cancer remains controversial. Here, we show that, in *Drosophila*, JNK has a tumor-suppressive role in a context of CF. JNK can control the expansion of cells with CF in at least two ways. It controls cell survival by regulating DIAP1, and cell proliferation by repressing Cdc25/stg in a context of *stg* overexpression. The overexpression of *yki* in cells with CF overcomes that tumor-suppressive barrier and promotes tumorigenesis by, presumably, upregulating cycle regulators such as Cyclin E and Stg, and by increasing the levels of DIAP1. Oncogenic Ras is also able to drive tumorous growth in cells with CF. Understanding whether Ras-V12 enhances Yki activity and, by doing so, drives tumor formation, or whether it uses an independent molecular pathway to trigger tumorigenesis in those cells, may merit further investigations.

Our results uncover a mechanism by which cells with defects in cytokinesis evolve to polyploidy and neoplasia. Polyploidy is normally found in some animal tissues including the liver. Notably, activation of YAP promotes oncogenesis in hepatocytes (Camargo et al., 2007; Dong et al., 2007; Zhang et al., 2017), and amplification of the inhibitor of apoptosis cIAP1 has been shown to accelerate tumorigenesis in the liver (Zender et al., 2006). Consistent with this, high-ploidy tumors show Hippo pathway inactivation and YAP amplification, compared to nearly diploid tumors (Ganem et al., 2014). Cancer is characterized by aberrant cell cycle, and cell cycle regulators are promising targets in cancer therapy. It would be interesting to study whether YAP controls Cdc25 expression in liver cells and to determine the role of Cdc25 in liver cancer (Xu et al., 2008; Xu et al., 2003).

EXPERIMENTAL PROCEDURES

Drosophila Strains

The following *Drosophila* strains are described in the cited references: *ap-Gal4* (Cohen et al., 1992), *hh-Gal4* (Calleja et al., 1996), *UAS-DIAP1* (Wang et al., 1999), *UAS-dpp* (Capdevila and Guerrero, 1994), *UAS-EGFR* (Buff et al., 1998), *UAS-Fly-FUCCI* (Zielke et al., 2014), *UAS-Notch-intra* (Doherty et al., 1996), *UAS-PI3K* (Leevers et al., 1996), *UAS-wg* (Klein and Arias, 1998), *UAS-yki* (Huang et al., 2005), *eyFLP, act > y^{+} > Gal4, UAS-GFP; FRT82B tub-Gal80* (Pagliarini and Xu, 2003), *FRT-wts^{X1}* (Xu et al., 1995), *TRE-RFP* (Chatterjee and Bohmann, 2012), *Cyclin E-lacZ* (Jones et al., 2000), *stg-lacZ (P{PZ}stg01235)* (Mitchell et al., 2013); *bantam-lacZ (P{lacW} banL1170a)* is described in FlyBase. The following stocks were provided by the Bloomington *Drosophila* Stock Center: *en-Gal4* (#1973), *UAS-Ras-V12* (#4847), *UAS-basket-DN* (#6409), *p53 5a-1-4* (#6815), *DIAP1-lacZ* (#12093), *Expanded^{697}-lacZ* (#44248), *four jointed-lacZ* (#44253), *UAS-ago-RNAi* (#34802), *UAS-avl-RNAi* (#29546), *UAS-Csk-RNAi* (#41712), *UAS-dia-RNAi* (#33424), *UAS-dlg1-RNAi* (#39035), *UAS-lgl-RNAi* (#38989), *UAS-Orbit-RNAi* (#34669), *UAS-p35* (#6298), *UAS-p53-DN* (#8420), *UAS-pbl-RNAi* (#28343), *UAS-scrib-RNAi* (#39073), *UAS-stg* (#56562), and *UAS-Tsc1-RNAi* (#54034). The following stocks were provided by the Vienna *Drosophila* RNAi Center: *UAS-Incenp-RNAi* (#17044), *UAS-pnut-RNAi* (#11791), *UAS-Pten-RNAi* (#101475), *UAS-Rab5-RNAi* (#34096), *UAS-tsg101-RNAi* (#23944), and *UAS-wts-RNAi* (#106174).

Gal4/Gal80TS System in the Wing Imaginal Disc

The *apterous* enhancer was used to express *Gal4* conditionally in the dorsal compartment of the wing imaginal disc. Gal80TS was used to allow UAS-driven transgene expression after temperature switch from 18°C to 29°C (Zeidler et al., 2004). All gene manipulation experiments used the *tubulin-Gal80TS* construct. *Drosophila* crosses laid eggs for 2 days at 18°C, and the larvae were maintained for 5 additional days at 18°C. Subsequently, the larvae were transferred to 29°C and maintained for 3–14 days. Third-instar wandering larvae were dissected and processed for staining using immunohistochemistry.

Immunohistochemistry

The following primary antibodies were used: rabbit anti-CNN (provided by T. Kaufmann); mouse anti-DIAP1 (provided by B. Hay); rabbit anti-Stg (provided by E.F. Wieschaus); rabbit anti-Yki (provided by D.J. Pan); mouse anti-β-Galactosidase, mouse anti-Dlg1, mouse anti-Mmp1, mouse anti-p53, and mouse anti-Pnut (Developmental Studies Hybridoma Bank); rabbit anti-phospho-JNK (Promega; V7931); and rabbit anti-Cas3-act (Cell Signaling Technology; no. 9661).

Dissection of third-instar larvae was performed in PBS. Samples were fixed in 4% formaldehyde solution for 20 min at room temperature, washed three times for 10 min in phosphate-buffered saline-tween (PBT), and blocked for 20 min in BBT. Subsequently, the samples were incubated in the first antibody diluted in PBT-BSA (BBT) at room temperature overnight and washed three times for 15 min in BBT the next morning. The secondary antibody and DAPI

diluted in BBT were added and incubated for 2 hr at room temperature. Samples were washed four times for 15 min in PBT and mounted in 90% glycerol with PBS containing 0.05% propyl gallate. Wing imaginal discs were imaged with a Leica SP8 confocal laser-scanning microscope. Images were processed with ImageJ and Adobe Photoshop CC.

Centrosome Quantification

Wing imaginal discs of third-instar larvae were stained against CNN to mark centrosomes in cells that undergo mitosis. Three-dimensional images were taken of the dorsal compartment of wing imaginal discs with a Leica SP8 confocal laser-scanning microscope. The number of centrosomes per cell was determined for 300 cells per genotype.

Wing Imaginal Disc Size Quantification

Wing imaginal discs of third-instar larvae were imaged with a Leica SP8 confocal laser-scanning microscope, and the size of the GFP-positive area with ImageJ was determined. For this purpose, a threshold was set to comprise the whole GFP-positive area of the organ with the option "Threshold." Subsequently, the size of 15 organs per genotype was determined with the option "Analyze Particles." Statistical significance was determined by unpaired t test with GraphPad Prism 7.

Activated Caspase 3 Signal Quantification

Wing imaginal discs were stained against activated form of Caspase 3 and were imaged with a Leica SP8 confocal laser-scanning microscope. Subsequently, the signal of activated form of Caspase 3 was determined with ImageJ. For this purpose, the overall intensity of activated form of Caspase 3 signal of 15 wing imaginal discs per genotype was determined by using the measurement "Mean Gray Value" in ImageJ. Statistical significance was determined by unpaired t test with GraphPad Prism 7.

In Situ Hybridization

In situ hybridization was according to the procedures described by Azpiazu and Frasch (1993). Probes for *in situ* hybridization were generated by PCR with the DIG DNA Labeling Kit (Roche) and detected with the DIG Nucleic Acid Detection Kit (Roche). Wing imaginal discs were mounted in glycerol and imaged with a Leica DM 5500B bright-field microscope.

Primer sequences were as follows: Stg-fw, GCGCCAGATTCTCCTCGTTT; Stg-rev, TAATACGACTCACTATAGGGGATTAAGGGGTCTGATTTCGGGATCGG; DIAP1-fw, GCATTCAAACCCACCAGTCGAC; and DIAP1-rev, TAATACGACTCACTATAGGGTAGGCTTACGATAACTGGCAGGC.

Flow Cytometry Analysis

Wing imaginal discs of third-instar larvae were dissected in PBS and dissociated with trypsin-EDTA solution for 45 min. The cells were fixed with 4% formaldehyde solution for 20 min and 70% ethanol for 2 hr. Following, the fixed cells were incubated with DAPI in PBT for 1 hr. Flow cytometry was used to determine fluorescence of DAPI, GFP, and RFP with a BD FACSAria Fusion. An integral/peak dot plot of DAPI fluorescence was used to exclude doublets.

EdU Incorporation and Signal Quantification

Wing imaginal discs of third-instar larvae were incubated in 300 μM EdU in PBS for 30 min. Samples were fixed in 4% formaldehyde solution for 20 min at room temperature, washed three times for 10 min in PBT, and blocked for 20 min in BBT. EdU detection was performed with the Click-iT EdU Alexa Fluor 488 Imaging Kit (Invitrogen) by incubating the samples for 1 hr with the reaction mix provided by the Imaging Kit. Subsequently, the samples were washed in BBT for 10 min and incubated with DAPI in BBT for 2 hr at room temperature. Samples were washed four times for 15 min in PBT and mounted in 90% glycerol with PBS containing 0.05% propyl gallate.

The wing pouch region of wing imaginal discs of third-instar larvae was imaged with a Leica SP8 confocal laser-scanning microscope and the EdU signal determined with ImageJ. For this purpose, the overall intensity of EdU signal of 10 wing imaginal discs per genotype was determined by using the measurement "Mean Gray Value" in ImageJ. Statistical significance was determined by unpaired t test with GraphPad Prism 7.

Whole Larvae Image

Whole larvae images were taken in the bright-field and green fluorescent channel with a Leica M165 FC stereomicroscope. Images were processed with ImageJ and Adobe Photoshop CC. An overlay of the bright-field and green fluorescent image was generated using the blend mode "Luminosity" (Opacity 70%) in Adobe Photoshop CC.

Invasion Assay

Wing imaginal discs of third-instar larvae were fixed and imaged with a Leica SP8 confocal laser-scanning microscope. The number of cell patches that invaded the anterior compartment in one focal plane was counted in 15 organs per genotype.

Western Blot

Third-instar wing imaginal discs of 20–40 larvae were dissected in protein extraction and immunoprecipitation buffer (RIPA; Sigma-Aldrich), and Complete Protease Inhibitor Cocktail (Roche) was added. The tissue was homogenized, centrifuged (15 min, 13,000 rpm), and the supernatant further used. Protein concentration was determined with the BCA Protein Assay (Thermo Fisher). 6 μg of protein was loaded per sample for the western blots. Antibody against String (provided by E.F. Wieschaus) and against Tubulin (Sigma; DM1A) was used to detect protein. Secondary horseradish peroxidase (HRP) goat anti-rabbit and goat anti-mouse antibodies (Dako) and the Pierce ECL Western Blotting Substrate (Thermo Fisher) were used to visualize protein.

SUPPLEMENTAL INFORMATION

Supplemental Information includes Supplemental Experimental Procedures, six figures, and one table and can be found with this article online at https://doi.org/10.1016/j.celrep.2018.04.006.

ACKNOWLEDGMENTS

We thank S.M. Cohen for his help in the design of the project; M.A. Visser for technical support; L. Quinn, J. Pastor-Pareja, E.F. Wieschaus, T. Kaufmann, B. Hay, and D.J. Pan for reagents; P. Jarabo for her comments on the manuscript; and the DSHB, VDRC, and BDSC for antibodies and fly strains. Work was supported by Grant "DISC-B" from the Danish Council for Strategic Research, by NovoNordisk Foundation Grant NNF12OC0000552, and by a grant from the Neye Foundation for genetic models for cancer gene discovery.

AUTHOR CONTRIBUTIONS

S.U.G., T.E., and H.H. conceived the project. S.U.G., T.E., and H.H. performed the experimental work. S.U.G., T.E., and H.H. wrote the manuscript and prepared the figures. All authors edited the manuscript. H.H. supervised all aspects of the project.

DECLARATION OF INTERESTS

The authors declare no competing interests.

Received: June 7, 2017
Revised: March 14, 2018
Accepted: March 30, 2018
Published: May 1, 2018

REFERENCES

Adams, R.R., Maiato, H., Earnshaw, W.C., and Carmena, M. (2001). Essential roles of *Drosophila* inner centromere protein (INCENP) and aurora B in histone H3 phosphorylation, metaphase chromosome alignment, kinetochore disjunction, and chromosome segregation. J. Cell Biol. *153*, 865–880.

Andreassen, P.R., Lohez, O.D., Lacroix, F.B., and Margolis, R.L. (2001). Tetraploid state induces p53-dependent arrest of nontransformed mammalian cells in G1. Mol. Biol. Cell *12*, 1315–1328.

Atkins, M., Potier, D., Romanelli, L., Jacobs, J., Mach, J., Hamaratoglu, F., Aerts, S., and Halder, G. (2016). An ectopic network of transcription factors regulated by Hippo signaling drives growth and invasion of a malignant tumor model. Curr. Biol. *26*, 2101–2113.

Azpiazu, N., and Frasch, M. (1993). *tinman* and *bagpipe*: two homeo box genes that determine cell fates in the dorsal mesoderm of *Drosophila*. Genes Dev. *7* (*7B*), 1325–1340.

Beaucher, M., Hersperger, E., Page-McCaw, A., and Shearn, A. (2007). Metastatic ability of *Drosophila* tumors depends on MMP activity. Dev. Biol. *303*, 625–634.

Bilder, D. (2004). Epithelial polarity and proliferation control: links from the *Drosophila* neoplastic tumor suppressors. Genes Dev. *18*, 1909–1925.

Bouldin, C.M., and Kimelman, D. (2014). Cdc25 and the importance of G2 control: insights from developmental biology. Cell Cycle *13*, 2165–2171.

Brace, J., Hsu, J., and Weiss, E.L. (2011). Mitotic exit control of the *Saccharomyces cerevisiae* Ndr/LATS kinase Cbk1 regulates daughter cell separation after cytokinesis. Mol. Cell. Biol. *31*, 721–735.

Brennecke, J., Hipfner, D.R., Stark, A., Russell, R.B., and Cohen, S.M. (2003). *bantam* encodes a developmentally regulated microRNA that controls cell proliferation and regulates the proapoptotic gene *hid* in *Drosophila*. Cell *113*, 25–36.

Brodsky, M.H., Nordstrom, W., Tsang, G., Kwan, E., Rubin, G.M., and Abrams, J.M. (2000). *Drosophila* p53 binds a damage response element at the reaper locus. Cell *101*, 103–113.

Buff, E., Carmena, A., Gisselbrecht, S., Jiménez, F., and Michelson, A.M. (1998). Signalling by the *Drosophila* epidermal growth factor receptor is required for the specification and diversification of embryonic muscle progenitors. Development *125*, 2075–2086.

Bui, D.A., Lee, W., White, A.E., Harper, J.W., Schackmann, R.C., Overholtzer, M., Selfors, L.M., and Brugge, J.S. (2016). Cytokinesis involves a nontranscriptional function of the Hippo pathway effector YAP. Sci. Signal. *9*, ra23.

Burds, A.A., Lutum, A.S., and Sorger, P.K. (2005). Generating chromosome instability through the simultaneous deletion of Mad2 and p53. Proc. Natl. Acad. Sci. USA *102*, 11296–11301.

Calleja, M., Moreno, E., Pelaz, S., and Morata, G. (1996). Visualization of gene expression in living adult *Drosophila*. Science *274*, 252–255.

Camargo, F.D., Gokhale, S., Johnnidis, J.B., Fu, D., Bell, G.W., Jaenisch, R., and Brummelkamp, T.R. (2007). YAP1 increases organ size and expands undifferentiated progenitor cells. Curr. Biol. *17*, 2054–2060.

Capdevila, J., and Guerrero, I. (1994). Targeted expression of the signaling molecule decapentaplegic induces pattern duplications and growth alterations in *Drosophila* wings. EMBO J. *13*, 4459–4468.

Chang, C.J., Goulding, S., Adams, R.R., Earnshaw, W.C., and Carmena, M. (2006). *Drosophila* Incenp is required for cytokinesis and asymmetric cell division during development of the nervous system. J. Cell Sci. *119*, 1144–1153.

Chatterjee, N., and Bohmann, D. (2012). A versatile ΦC31 based reporter system for measuring AP-1 and Nrf2 signaling in *Drosophila* and in tissue culture. PLoS One *7*, e34063.

Cho, E., Feng, Y., Rauskolb, C., Maitra, S., Fehon, R., and Irvine, K.D. (2006). Delineation of a Fat tumor suppressor pathway. Nat. Genet. *38*, 1142–1150.

Cohen, B., McGuffin, M.E., Pfeifle, C., Segal, D., and Cohen, S.M. (1992). *apterous*, a gene required for imaginal disc development in *Drosophila* encodes a member of the LIM family of developmental regulatory proteins. Genes Dev. *6*, 715–729.

Dekanty, A., Barrio, L., Muzzopappa, M., Auer, H., and Milán, M. (2012). Aneuploidy-induced delaminating cells drive tumorigenesis in *Drosophila* epithelia. Proc. Natl. Acad. Sci. USA *109*, 20549–20554.

Doherty, D., Feger, G., Younger-Shepherd, S., Jan, L.Y., and Jan, Y.N. (1996). Delta is a ventral to dorsal signal complementary to Serrate, another Notch ligand, in *Drosophila* wing formation. Genes Dev. *10*, 421–434.

Dong, J., Feldmann, G., Huang, J., Wu, S., Zhang, N., Comerford, S.A., Gayyed, M.F., Anders, R.A., Maitra, A., and Pan, D. (2007). Elucidation of a universal size-control mechanism in *Drosophila* and mammals. Cell *130*, 1120–1133.

Eichenlaub, T., Cohen, S.M., and Herranz, H. (2016). Cell competition drives the formation of metastatic tumors in a *Drosophila* model of epithelial tumor formation. Curr. Biol. *26*, 419–427.

Fausto, N., and Campbell, J.S. (2003). The role of hepatocytes and oval cells in liver regeneration and repopulation. Mech. Dev. *120*, 117–130.

Florindo, C., Perdigão, J., Fesquet, D., Schiebel, E., Pines, J., and Tavares, A.A. (2012). Human Mob1 proteins are required for cytokinesis by controlling microtubule stability. J. Cell Sci. *125*, 3085–3090.

Fujiwara, T., Bandi, M., Nitta, M., Ivanova, E.V., Bronson, R.T., and Pellman, D. (2005). Cytokinesis failure generating tetraploids promotes tumorigenesis in p53-null cells. Nature *437*, 1043–1047.

Ganem, N.J., Godinho, S.A., and Pellman, D. (2009). A mechanism linking extra centrosomes to chromosomal instability. Nature *460*, 278–282.

Ganem, N.J., Cornils, H., Chiu, S.Y., O'Rourke, K.P., Arnaud, J., Yimlamai, D., Théry, M., Camargo, F.D., and Pellman, D. (2014). Cytokinesis failure triggers hippo tumor suppressor pathway activation. Cell *158*, 833–848.

Goulev, Y., Fauny, J.D., Gonzalez-Marti, B., Flagiello, D., Silber, J., and Zider, A. (2008). SCALLOPED interacts with YORKIE, the nuclear effector of the hippo tumor-suppressor pathway in *Drosophila*. Curr. Biol. *18*, 435–441.

Green, R.A., Paluch, E., and Oegema, K. (2012). Cytokinesis in animal cells. Annu. Rev. Cell Dev. Biol. *28*, 29–58.

Gutierrez, G.J., Tsuji, T., Cross, J.V., Davis, R.J., Templeton, D.J., Jiang, W., and Ronai, Z.A. (2010). JNK-mediated phosphorylation of Cdc25C regulates cell cycle entry and G_2/M DNA damage checkpoint. J. Biol. Chem. *285*, 14217–14228.

Hamaratoglu, F., Willecke, M., Kango-Singh, M., Nolo, R., Hyun, E., Tao, C., Jafar-Nejad, H., and Halder, G. (2006). The tumour-suppressor genes NF2/Merlin and Expanded act through Hippo signalling to regulate cell proliferation and apoptosis. Nat. Cell Biol. *8*, 27–36.

Hay, B.A., and Guo, M. (2006). Caspase-dependent cell death in *Drosophila*. Annu. Rev. Cell Dev. Biol. *22*, 623–650.

Herranz, H., Eichenlaub, T., and Cohen, S.M. (2016). Cancer in *Drosophila*: imaginal discs as a model for epithelial tumor formation. Curr. Top. Dev. Biol. *116*, 181–199.

Huang, J., Wu, S., Barrera, J., Matthews, K., and Pan, D. (2005). The Hippo signaling pathway coordinately regulates cell proliferation and apoptosis by inactivating Yorkie, the *Drosophila* homolog of YAP. Cell *122*, 421–434.

Inoue, Y.H., Savoian, M.S., Suzuki, T., Máthé, E., Yamamoto, M.T., and Glover, D.M. (2004). Mutations in orbit/mast reveal that the central spindle is comprised of two microtubule populations, those that initiate cleavage and those that propagate furrow ingression. J. Cell Biol. *166*, 49–60.

Jones, L., Richardson, H., and Saint, R. (2000). Tissue-specific regulation of cyclin E transcription during *Drosophila melanogaster* embryogenesis. Development *127*, 4619–4630.

Kanda, H., and Miura, M. (2004). Regulatory roles of JNK in programmed cell death. J. Biochem. *136*, 1–6.

Klein, T., and Arias, A.M. (1998). Different spatial and temporal interactions between Notch, wingless, and vestigial specify proximal and distal pattern elements of the wing in *Drosophila*. Dev. Biol. *194*, 196–212.

Kuffer, C., Kuznetsova, A.Y., and Storchová, Z. (2013). Abnormal mitosis triggers p53-dependent cell cycle arrest in human tetraploid cells. Chromosoma *122*, 305–318.

Lanni, J.S., and Jacks, T. (1998). Characterization of the p53-dependent postmitotic checkpoint following spindle disruption. Mol. Cell. Biol. *18*, 1055–1064.

Leevers, S.J., Weinkove, D., MacDougall, L.K., Hafen, E., and Waterfield, M.D. (1996). The *Drosophila* phosphoinositide 3-kinase Dp110 promotes cell growth. EMBO J. *15*, 6584–6594.

Li, M., Fang, X., Baker, D.J., Guo, L., Gao, X., Wei, Z., Han, S., van Deursen, J.M., and Zhang, P. (2010). The ATM-p53 pathway suppresses aneuploidy-induced tumorigenesis. Proc. Natl. Acad. Sci. USA *107*, 14188–14193.

Mann, R.S., and Morata, G. (2000). The developmental and molecular biology of genes that subdivide the body of *Drosophila*. Annu. Rev. Cell Dev. Biol. *16*, 243–271.

Minn, A.J., Boise, L.H., and Thompson, C.B. (1996). Expression of Bcl-xL and loss of p53 can cooperate to overcome a cell cycle checkpoint induced by mitotic spindle damage. Genes Dev. *10*, 2621–2631.

Mitchell, N.C., Lin, J.I., Zaytseva, O., Cranna, N., Lee, A., and Quinn, L.M. (2013). The Ecdysone receptor constrains wingless expression to pattern cell cycle across the *Drosophila* wing margin in a Cyclin B-dependent manner. BMC Dev. Biol. *13*, 28.

Morais da Silva, S., Moutinho-Santos, T., and Sunkel, C.E. (2013). A tumor suppressor role of the Bub3 spindle checkpoint protein after apoptosis inhibition. J. Cell Biol. *201*, 385–393.

Mukai, S., Yabuta, N., Yoshida, K., Okamoto, A., Miura, D., Furuta, Y., Abe, T., and Nojima, H. (2015). Lats1 suppresses centrosome overduplication by modulating the stability of Cdc25B. Sci. Rep. *5*, 16173.

Muro, I., Hay, B.A., and Clem, R.J. (2002). The *Drosophila* DIAP1 protein is required to prevent accumulation of a continuously generated, processed form of the apical caspase DRONC. J. Biol. Chem. *277*, 49644–49650.

Neufeld, T.P., and Rubin, G.M. (1994). The *Drosophila* peanut gene is required for cytokinesis and encodes a protein similar to yeast putative bud neck filament proteins. Cell *77*, 371–379.

Pagliarini, R.A., and Xu, T. (2003). A genetic screen in *Drosophila* for metastatic behavior. Science *302*, 1227–1231.

Pan, D. (2010). The hippo signaling pathway in development and cancer. Dev. Cell *19*, 491–505.

Prokopenko, S.N., Brumby, A., O'Keefe, L., Prior, L., He, Y., Saint, R., and Bellen, H.J. (1999). A putative exchange factor for Rho1 GTPase is required for initiation of cytokinesis in *Drosophila*. Genes Dev. *13*, 2301–2314.

Reis, T., and Edgar, B.A. (2004). Negative regulation of dE2F1 by cyclin-dependent kinases controls cell cycle timing. Cell *117*, 253–264.

Sakaue-Sawano, A., Kurokawa, H., Morimura, T., Hanyu, A., Hama, H., Osawa, H., Kashiwagi, S., Fukami, K., Miyata, T., Miyoshi, H., et al. (2008). Visualizing spatiotemporal dynamics of multicellular cell-cycle progression. Cell *132*, 487–498.

Schvartzman, J.M., Sotillo, R., and Benezra, R. (2010). Mitotic chromosomal instability and cancer: mouse modelling of the human disease. Nat. Rev. Cancer *10*, 102–115.

Silkworth, W.T., Nardi, I.K., Scholl, L.M., and Cimini, D. (2009). Multipolar spindle pole coalescence is a major source of kinetochore mis-attachment and chromosome mis-segregation in cancer cells. PLoS One *4*, e6564.

Uchida, S., Yoshioka, K., Kizu, R., Nakagama, H., Matsunaga, T., Ishizaka, Y., Poon, R.Y., and Yamashita, K. (2009). Stress-activated mitogen-activated protein kinases c-Jun NH2-terminal kinase and p38 target Cdc25B for degradation. Cancer Res. *69*, 6438–6444.

Udan, R.S., Kango-Singh, M., Nolo, R., Tao, C., and Halder, G. (2003). Hippo promotes proliferation arrest and apoptosis in the Salvador/Warts pathway. Nat. Cell Biol. *5*, 914–920.

Uetake, Y., and Sluder, G. (2004). Cell cycle progression after cleavage failure: mammalian somatic cells do not possess a "tetraploidy checkpoint.". J. Cell Biol. *165*, 609–615.

Uhlirova, M., and Bohmann, D. (2006). JNK- and Fos-regulated Mmp1 expression cooperates with Ras to induce invasive tumors in *Drosophila*. EMBO J. *25*, 5294–5304.

Uhlirova, M., Jasper, H., and Bohmann, D. (2005). Non-cell-autonomous induction of tissue overgrowth by JNK/Ras cooperation in a *Drosophila* tumor model. Proc. Natl. Acad. Sci. USA *102*, 13123–13128.

Verghese, S., and Su, T.T. (2016). *Drosophila* Wnt and STAT define apoptosis-resistant epithelial cells for tissue regeneration after irradiation. PLoS Biol. *14*, e1002536.

Vidal, M., Larson, D.E., and Cagan, R.L. (2006). Csk-deficient boundary cells are eliminated from normal *Drosophila* epithelia by exclusion, migration, and apoptosis. Dev. Cell *10*, 33–44.

Wang, S.L., Hawkins, C.J., Yoo, S.J., Müller, H.A., and Hay, B.A. (1999). The *Drosophila* caspase inhibitor DIAP1 is essential for cell survival and is negatively regulated by HID. Cell *98*, 453–463.

Wasserman, S. (1998). FH proteins as cytoskeletal organizers. Trends Cell Biol. *8*, 111–115.

Willsey, H.R., Zheng, X., Carlos Pastor-Pareja, J., Willsey, A.J., Beachy, P.A., and Xu, T. (2016). Localized JNK signaling regulates organ size during development. eLife *5*, e11491.

Wu, S., Huang, J., Dong, J., and Pan, D. (2003). *hippo* encodes a Ste-20 family protein kinase that restricts cell proliferation and promotes apoptosis in conjunction with *salvador* and *warts*. Cell *114*, 445–456.

Wu, S., Liu, Y., Zheng, Y., Dong, J., and Pan, D. (2008). The TEAD/TEF family protein Scalloped mediates transcriptional output of the Hippo growth-regulatory pathway. Dev. Cell *14*, 388–398.

Xu, T., Wang, W., Zhang, S., Stewart, R.A., and Yu, W. (1995). Identifying tumor suppressors in genetic mosaics: the *Drosophila lats* gene encodes a putative protein kinase. Development *121*, 1053–1063.

Xu, X., Yamamoto, H., Sakon, M., Yasui, M., Ngan, C.Y., Fukunaga, H., Morita, T., Ogawa, M., Nagano, H., Nakamori, S., et al. (2003). Overexpression of CDC25A phosphatase is associated with hypergrowth activity and poor prognosis of human hepatocellular carcinomas. Clin. Cancer Res. *9*, 1764–1772.

Xu, X., Yamamoto, H., Liu, G., Ito, Y., Ngan, C.Y., Kondo, M., Nagano, H., Dono, K., Sekimoto, M., and Monden, M. (2008). CDC25A inhibition suppresses the growth and invasion of human hepatocellular carcinoma cells. Int. J. Mol. Med. *21*, 145–152.

Yabuta, N., Yoshida, K., Mukai, S., Kato, Y., Torigata, K., and Nojima, H. (2016). Large tumor suppressors 1 and 2 regulate Aurora-B through phosphorylation of INCENP to ensure completion of cytokinesis. Heliyon *2*, e00131.

Zack, T.I., Schumacher, S.E., Carter, S.L., Cherniack, A.D., Saksena, G., Tabak, B., Lawrence, M.S., Zhsng, C.Z., Wala, J., Mermel, C.H., et al. (2013). Pan-cancer patterns of somatic copy number alteration. Nat. Genet. *45*, 1134–1140.

Zeidler, M.P., Tan, C., Bellaiche, Y., Cherry, S., Häder, S., Gayko, U., and Perrimon, N. (2004). Temperature-sensitive control of protein activity by conditionally splicing inteins. Nat. Biotechnol. *22*, 871–876.

Zender, L., Spector, M.S., Xue, W., Flemming, P., Cordon-Cardo, C., Silke, J., Fan, S.T., Luk, J.M., Wigler, M., Hannon, G.J., et al. (2006). Identification and validation of oncogenes in liver cancer using an integrative oncogenomic approach. Cell *125*, 1253–1267.

Zhang, L., Ren, F., Zhang, Q., Chen, Y., Wang, B., and Jiang, J. (2008). The TEAD/TEF family of transcription factor Scalloped mediates Hippo signaling in organ size control. Dev. Cell *14*, 377–387.

Zhang, S., Chen, Q., Liu, Q., Li, Y., Sun, X., Hong, L., Ji, S., Liu, C., Geng, J., Zhang, W., et al. (2017). Hippo Signaling Suppresses Cell Ploidy and Tumorigenesis through Skp2. Cancer Cell *31*, 669–684.e7.

Zielke, N., Korzelius, J., van Straaten, M., Bender, K., Schuhknecht, G.F., Dutta, D., Xiang, J., and Edgar, B.A. (2014). Fly-FUCCI: a versatile tool for studying cell proliferation in complex tissues. Cell Rep. *7*, 588–598.